A Modelling Approach for Predicting Marine Engines Shaft Dynamics

K M Tsitsilonis, MEng, MIMarEST[a,b*], Dr. G Theotokatos FIMarEST[a], M Habens, MIMarEST[b]
[a]*Maritime Safety Research Centre, Department of Naval Architecture, Ocean & Marine Engineering, University of Strathclyde, 100 Montrose Street, Glasgow G4 0LZ, UK;*
[b]*Datum Electronics Ltd., Castle St, East Cowes PO32 6EZ, UK*
*Corresponding author. Email: konstantinos.tsitsilonis@strath.ac.uk

Synopsis

For making decisions on maintenance and operations of ship systems in a timely and cost effective way, intelligent approaches for continuously assessing the critical ship systems condition are required. This study aims to provide a framework for large marine two-stroke diesel engines performance assessment, by mapping the relationship of specific malfunctioning engine conditions on the Instantaneous Crankshaft Torque (ICT). This is accomplished by the development of a thermodynamics model, which is coupled with a lumped mass crankshaft dynamics model, in order to predict the engine shaft dynamics and torsional response. Subsequently, by employing the coupled engine models, a number of case studies are simulated for investigating the influence on the engine ICT, which include: (**a**) change in the Start of Injection (SOI), (**b**) change in the Rate of Heat Release (RHR), (**c**) change in the scavenge air pressure, and (**d**) leaking exhaust valve. By investigating the predicted ICT from the coupled model in both the time and frequency domains, distinct frequencies are identified, which correspond to specific engine malfunctioning conditions. Based on the derived results, these engine malfunctioning conditions are mapped with the frequencies most affected in the engine's instantaneous torque, which demonstrate the usefulness of implementing the the ICT measurement for diagnostic purposes.

Keywords: Malfunctions engine conditions mapping; Engine maintenance; Shafting dynamics; Lumped-mass model; Two-stroke internal combustion engine.

1 Introduction

Two-stroke diesel engines are highly efficient and reliable internal combustion engines, and as a result they are employed as the main engines for over 85% of the world merchant fleet (Anantharaman et al., 2015). However, main engine breakdown is amongst the most frequent and expensive insurance claims (The Swedish Club, 2018), thus faults which lead to breakdowns of such engines can be costly to operators and insurers alike, as well as critical to the vessel safety (Matulić et al., 2019). In addition, the engine components fouling and degradation result in lower operational efficiency, which is associated with higher fuel consumption and operating cost. Consequently, early diagnosis of engine abnormalities, degradation and faults is key in maintaining the vessel's safety, as well as avoiding higher operational expenditure associated with fuel, maintenance, costly downtime and increased repair costs.

In order to diagnose the engine condition, monitoring of key engine parameters is firstly required. One of the parameters that characterises the engine health status is the in-cylinder pressure (Heywood, 1988; Martyr and Plint, 2012). However, measuring the in-cylinder pressure is intrusive, and due to the sensors limited life, it cannot be performed in a continuous basis (Woodyard, 2009; Martyr and Plint, 2012), which is vital for effective diagnosing and early fault detection. To overcome these shortcomings, other performance parameters are continuously monitored from the engine monitoring system, such as the cylinders exhaust gas temperature and the scavenging receiver pressure. However, they may be less revealing regarding the engine cylinders' health status. Additionally, by monitoring a greater number of parameters, a more extensive sensor network is required, which increases the cost of monitoring, introduces multiple sensor failure points, and may cause synchronisation issues (Isermann, 2006). Considering the recent advances in the strain gauging and data storage technologies, the measurement of the engine's Instantaneous Crankshaft Torque (ICT) can be readily obtained, thus providing information for the

Authors' Biographies

Konstantinos - Marios Tsitsilonis is currently the Lead Marine Project Engineer in Datum Electronics, and a PhD researcher at the Maritime Safety Research Centre of Strathclyde University. He begun his research career in offshore drillship energy management projects at CIMC Raffles, Yantai, and continued working in the field as a research assistant. He subsequently went on to perform scrubber retrofits in numerous vessels, before returning to research and development on maintenance and diagnostics of internal combustion engines.

Dr. Gerasimos Theotokatos is the DNV GL Reader on Safety of Marine Systems at the Maritime Safety Research Centre of Strathclyde University, and has obtained a PhD degree from NTUA in 2001, in the discipline of Marine Engineering. His research focuses on the development of scientific approaches to holistically capture the safety, energy and sustainability interplay of the complex marine systems including cyber-physical and autonomous systems by employing advanced model-based methods and tools for the design and optimisation of marine systems.

Malcolm Habens has worked in the strain measurement industry for over 40 years with British Hovercraft Electronic Labs, ITT, LCM Systems and Strainstall before founding Datum Electronics in 1989. Malcolm has designed many variants of strain sensors use in both static and rotary systems. He has worked on the analysis of dynamic strain data from rotary machinery including mixers, gearbox test rigs and diesel generators. Work in the later are has resulted in a patent application for advanced diesel engine monitoring.

 https://doi.org/10.24868/issn.2515-818X.2020.033

condition of all cylinders by deploying a single sensor (Schagerberg and McKelvey, 2003; Guerrero and Jiménez-Espadafor, 2019).

In specific, the above has been demonstrated in the literature for automotive applications, where the ICT measurement has been utilised to estimate combustion properties (Thor et al., 2014), and the peak pressure position (Larsson and Schagerberg, 2004) for each engine cylinder. In addition, regarding two-stroke diesel engines, the ICT measurement was used to estimate the indicated power of each cylinder (Guerrero and Jiménez-Espadafor, 2019), and to demonstrate relationships between the engine torque harmonic frequencies and the engine operating point (Espadafor et al., 2014). Despite of the these applications, utilisation of the ICT measurement for diagnostic purposes is still a novel concept for the shipping industry, which is a result of the *energy efficiency gap* that exists in the shipping industry (Johnson and Andersson, 2014). This is bound to improve due to greater and faster access to digital information, as well as improved flexibility in the shipping industry corporate structures (Lambrou et al., 2019).

In the shipping industry, the most basic form of diagnostics relies on human expertise in combination with information on acceptable tolerances of engine performance parameters provided by the manufacturers (MAN B&W). This is however a manual, non-continuous and error-prone method of fault diagnosis due to the extensive involvement of the human factor. Due to technological advances in data storage and transmission technologies, statistical diagnostics techniques can be implemented (Mesbahi et al., 2004; Raptodimos and Lazakis, 2018; Cai et al., 2017). However, these usually rely on the collection of data training sets from large sensor networks, which have to include healthy and most importantly unhealthy engine conditions, the latter of which may be difficult to obtain. The amount of measured parameters can be reduced by introducing modelling techniques, which can predict key engine parameters for the purposes of fault identification. In specific, thermodynamics modelling in conjunction with measured parameters has been extensively used by constructing a baseline in order to identify faults, such as excessive maximum combustion pressure (Kouremenos and Hountalas, 1997), cylinder blowby and compression faults (Watzenig et al., 2009), as well as changes in injection timing (Lamaris and Hountalas, 2010).

Therefore, this study aims to provide a framework for large two-stroke diesel engine performance assessment, by mapping the relationship of specific malfunctioning engine conditions and the ICT. This is performed by coupling together the validated engine thermodynamics and crankshaft dynamics models, so that the effect of specific simulated malfunctioning engine conditions on the engine's ICT is predicted. Subsequently, a frequency analysis on the ICT is performed, so that the unique frequencies affected by the investigated malfunctioning conditions, which are introduced in individual cylinders, are identified. In specific, the following frequently faced malfunctioning conditions are considered (Kouremenos and Hountalas, 1997; Benvenuto and Campora, 2007; Lamaris and Hountalas, 2010):

1. Change in Start of Injection (SOI).
2. Change in the Rate of Heat Release (RHR).
3. Change in the scavenge air pressure.
4. Leaking exhaust gas.

2 Methodology & Reference System

The engine employed for this study is a ten cylinder two-stroke diesel stationary generator, with its technical features listed in Table 1. The engine operation at healthy conditions is simulated and calibrated using a coupled thermodynamics and crankshaft dynamics model, which is configurable for stationary and propulsion applications. The engine operation is simulated for 100% engine load, with data obtained from Guerrero and Jiménez-Espadafor (2019). The output obtained from the coupled engine model is the in-cylinder pressure and the ICT.

Subsequently, the the simulation of the engine malfunctioning conditions listed at the end of Section 1 is carried out by the means of parametric runs. In specific, for every individual cylinder, 4 model parameters are used to simulate the malfunctioning conditions. These parameters are changed one at a time, where a total of 5 simulation runs are performed per parameter to uniformly cover the entire range of values, which is defined in Section 3.3. Finally, an extra simulation run is performed at healthy engine conditions, which is used as the baseline.

Thus, 5 parametric runs are performed for the first 3 malfunctioning conditions which are; change in SOI, change in RHR and leaking exhaust gas valve for each cylinder. This provides a total of 15 runs per cylinder, and a total of 150 runs for all 10 cylinders. In addition, the malfunctioning condition of change in scavenge air pressure is implemented to all cylinders simultaneously, which results to an additional 5 runs. By including the baseline run as well, this provides a total of 156 simulation runs. From the derived results of these runs, the difference in ICT from the baseline is calculated and analysed by using a discrete Fourier transform, in order to examine and map the effect of individual cylinder malfunctioning conditions.

 https://doi.org/10.24868/issn.2515-818X.2020.033

Table 1: Reference engine basic characteristics.

No. of cylinders	10
Nominal speed	125 rpm
Maximum continuous rating	15.5 MW
Cylinder bore	0.67 m

3 Modelling

3.1 Engine Thermodynamics Model

An in-house zero-dimensional thermodynamic model was employed for the calculation of the engine cylinder parameters variations considering both healthy and faulty/degraded conditions. This model is developed in Matlab/Simulink (Figure 1) and has been used to predict the performance of various two-stroke engines in both steady state and transient conditions. The model is described in detail in Guan et al. (2015).

In this study, one complete engine cylinder block including the scavenging ports and exhaust valve is modelled. The engine cylinder processes were modelled by using the zero-dimensional approach that employs the energy and mass conservation equations along with the ideal gas equation for the calculation of the cylinders working media temperature, mass, pressure and mixture composition. An one zone approach was used for modelling the closed cycle (compression, combustion, expansion) and the exhaust blow down, whereas a two-zone approach is used for modelling the scavenging process (from the scavenging port open to the exhaust valve close). The cylinder gas to wall heat transfer coefficient was calculated by employing the Woschni equation (Woschni, 1967). The Chen-Flynn friction model (Rakopoulos and Giakoumis, 2007) was employed for calculating the engine friction mean effective pressure. The combustion model employs the Woschni-Annisits model with a single Wiebe function to calculate the heat release rate, whereas the Sitkey equation is used for the calculation of the injection delay (Merker et al., 2005). The cumulative burned fuel is calculated according to the following Equation:

$$x_b = 1 - \exp\left\{-\alpha\left(\frac{\theta - \theta_{SC}}{\Delta\theta}\right)^{m+1}\right\} \tag{1}$$

where α is the Wiebe function parameter; θ denotes the crank angle, θ_{SC} denotes the crank angle at the start of combustion; $\Delta\theta$ is the combustion duration and m denotes the Wiebe function shape factor.

The mass flow rates through the engine intake and exhaust valves are calculated by using the quasi-steady adiabatic flow equation considering the respective profiles (equivalent area versus crank angle) and pressure ratios (Heywood, 1988). The engine crank shaft rotational speed is modelled by employing the angular momentum conservation equation.

The engine inlet and exhaust manifolds were modelled by using fixed fluid elements, providing the pressure, temperature and composition of the working media (air or exhaust gas) as input. The model parameters were calibrated to represent with sufficient accuracy the engine measured data and then employed for the investigated parametric runs with various abnormal/degraded conditions in this study.

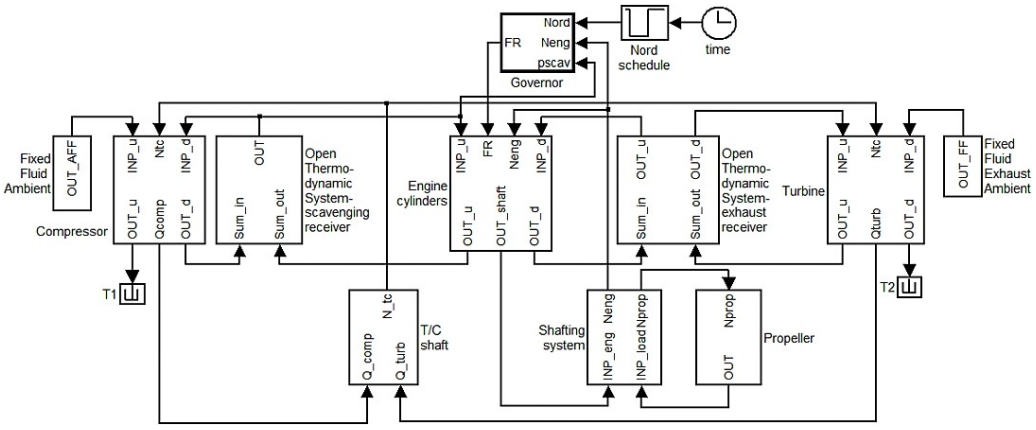

Figure 1: Thermodynamics model.

 https://doi.org/10.24868/issn.2515-818X.2020.033

3.2 Engine Crankshaft Dynamics Model

The above thermodynamics model was coupled with a crankshaft dynamics model, which can be configured to predict the engine ICT for either a stationary generator plant, or a propulsion plant. In specific, the engine's crankshaft is modelled by employing a lumped mass model as shown in Figure 2, which represents the engine crankshaft as a number of discrete inertia disks. For the investigated system, out of the total of 16 inertia disks, the 10 correspond to the crankthrow and piston assembly of each cylinder, whereas the remaining six correspond to the torsional vibration dampers, chaindrive, flywheel and engine load. The inertia disks are connected to each other with torsional springs and damper elements to simulate the shafting system's flexibility and structural damping. In addition, each mass is connected to a non-rotating frame of reference or ground with a damper element in order to simulate engine friction. Subsequently, the shafting system's governing equation of motion is formulated as follows:

$$\boldsymbol{J}\ddot{\Theta}+\boldsymbol{C}\dot{\Theta}+\boldsymbol{K}\Theta=\boldsymbol{T}_j(\ddot{\Theta},\dot{\Theta},\Theta)+\boldsymbol{T}_f(\dot{\Theta})+\boldsymbol{T}_c(\Theta)+\boldsymbol{T}_L \tag{2}$$

where $\boldsymbol{J}$, $\boldsymbol{C}$ and $\boldsymbol{K}$ are 16×16 inertia, damping and stiffness matrices; Θ, $\dot{\Theta}$ and $\ddot{\Theta}$ are 16×1 vectors of the instantaneous angular displacement, engine speed and acceleration; $\boldsymbol{T}_j$, $\boldsymbol{T}_f$, $\boldsymbol{T}_c$, and $\boldsymbol{T}_L$ are vector valued functions of the variable inertia, bearings friction, cylinder combustion and engine load torques respectively. Depending on whether the model is configured for a stationary generator or a propulsion engine, the load is either considered as a constant (Espadafor et al., 2014), or is derived in accordance to the propeller law (MAN Energy Solutions, 2018) using the following equations:

$$T_{L,\text{gen}}=\mathrm{k}\frac{P_{MCR}}{\dot{\theta}_{MCR}} \tag{3}$$

$$T_{L,\text{prop}}=k_q\dot{\theta}^n \quad \text{where } k_q=\frac{P_{MCR}}{\dot{\theta}_{MCR}^{n+1}} \tag{4}$$

where P_{MCR} is the engine power at the engine Maximum Continuous Rating (MCR), $\dot{\theta}_{MCR}$ is the engine speed at MCR, k is the generator load constant which is obtained from on-site bus voltage measurements (Espadafor et al., 2014), and $n\approx2$ is the propeller law exponent (MAN Energy Solutions, 2018). The engine load is implemented in the model as the last element of the engine load vector; $\boldsymbol{T}_L=[0,0,\cdots T_L]^{\mathrm{T}}$.

The variable inertia terms are modelled using the constant inertia-speed approach (Schagerberg and McKelvey, 2003). This simplifies the term $\boldsymbol{T}_j$ by replacing first the instantaneous engine speed with the engine's average speed, and second the variable inertia of the crankthrow and lower part of the connecting rod, by its average value within one revolution. In addition, the engine bearings friction torque is modelled as being proportional to the instantaneous engine speed, and the engine load is assumed constant. The model is described in further detail in Tsitsilonis et al. (2020).

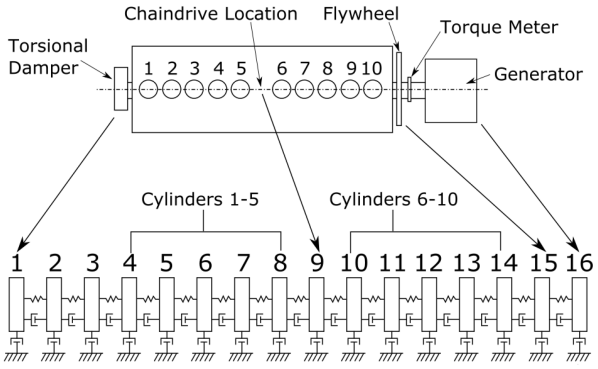

Figure 2: Crankshaft dynamics model (Tsitsilonis et al., 2020).

3.3 Engine Malfunctioning Condition Modelling

There have been a total of 4 engine malfunctioning conditions chosen to be modelled, so that their effect on the engine's shaft ICT is predicted. The first is the implementation of a change in the SOI, which typically caused in the variable injection timing (VIT) of the individual cylinders that might require re-tuning (Lamaris and Hountalas, 2010), or by the wear and tear of the camshaft lobe or the injector pump. The latter occurs in a large percentage of the world fleet, which still operates using camshaft-driven engines. Thus, the SOI angle for each cylinder (θ_{SOI}) can be changed by considering that the start of combustion angle from Equation 1, which is equivalent to:

$$\theta_{SC}=\theta_{SOI}+\theta_{\text{delay}} \tag{5}$$

 https://doi.org/10.24868/issn.2515-818X.2020.033

It is expected that there is a variation in timing of $\pm 4.5^{\circ}$CA (Hountalas, 2000), thus θ_{SOI} is changed accordingly.

The second malfunctioning condition is the implementation of a change in the RHR, which can be caused by a number of factors such as different fuel quality, worn injectors, or clogged injectors (Merker et al., 2005). Subsequently, this is modelled by increasing or decreasing the value of the Weibe shape parameter (m) in Equation 1. In specific, since the model is very sensitive to changes in the Weibe shape parameter, its value is changed by ± 1.5 with respect to the healthy engine's parameter value.

The third malfunctioning condition is a change in the scavenge air pressure. A decrease in the scavenge air pressure can occur primarily due to either turbocharger compressor wear, fouled turbocharger filter, fouled air cooler, or a combination of the above. In contrast, an increase in the scavenge air pressure can take place due to blockage in the turbine nozzle from fouling, or due to higher exhaust gas temperatures caused by the incomplete combustion of lower fuel quality (Tsitsilonis and Theotokatos, 2018). In this case, the scavenge air pressure was altered by ± 0.2 bar with respect to the healthy engine's scavenge air pressure.

The fourth malfunctioning condition is a exhaust valve leakage, which is caused due to deposits and/or lack of maintenance, and results in an imperfect seal when the exhaust valve closes. This was modelled by considering the exhaust valve effective area profile as a function of crank angle $A_e(\theta)$, which is 0 when the valve is closed, and reaches a maximum when the valve is fully open. Therefore, the valve's effective area profile was modified by limiting the minimum value of the valve profile such in accordance to the following equation:

$$A_{e,l}(\theta) = \max\{A_e(\theta), A_l\} \tag{6}$$

where A_l is the leaking surface area of the valve. This area was chosen to be 0.5% of the maximum exhaust valve effective area, i.e. $A_l = 0.05 \max\{A_e(\theta)\}$.

The modelled malfunctioning conditions and their respective parameters changes are summarised in Table 2.

Table 2: Malfunctioning conditions parameters variation.

Malfunctioning Condition	Changed Parameter	Parameter Range	Parameter Step
Change in SOI	Start of Combustion (θ_{SOI})	$\pm 4.5^{\circ}$	2.25°
Change in RHR	Weibe shape parameter (m)	± 1.5	0.75
Change in scanvenge air pressure	Scavenge air pressure (P_{scav})	± 0.2 bar	0.1 bar
Exhaust valve leak	Exhaust valve effective area (A_e)	$0 \sim 0.5\%$	0.124%

4 Results & Discussion

4.1 Healthy Engine Condition

The coupled thermodynamics and crankshaft dynamics model was calibrated accordingly for the 100% engine load operating point, such that its output matched the measured in-cylinder pressure for cylinder 1 and ICT data that were made available from Guerrero and Jiménez-Espadafor (2019), as presented in Figure 3. The Normalised Mean Square Error (NRMSE) of the model output in comparison to the measured data is 1.2% and 8.10% for the in-cylinder pressure of cylinder 1 and the ICT, respectively. The NRMSE is significantly higher for the case of the engine shaft ICT. This is attributed to the fact that unlike the model, where the in-cylinder pressure was assumed to be identical for all cylinders to simulate healthy conditions, when the ICT measurement was recorded the in-cylinder pressures were most likely different across the cylinders. Subsequently,this justifies the larger difference in NRMSE for the case of the ICT measured data. Further discussion on the above is available in Tsitsilonis et al. (2020).

Regarding the ICT of the engine it is interesting to note that even though the engine has 10 cylinders, only 5 peaks observed in the ICT. In specific, as observed in Figure 3, a cylinder is firing at either side of each peak in the engine ICT. The fact that the 10 peaks do not appear in the engine ICT can be attributed to the large moment of inertia of the generator, which is two orders of magnitude larger than the inertia of any other part of the shafting system. Subsequently the generator is responsible for introducing significant effects into the dynamics of the system, by making the shafting system behave approximately as if it consisted of only two inertia disks (the inertia disk of the complete engine crankshaft including the flywheel, and the inertia disk of the electric generator).

4.2 Engine Malfunctioning Conditions Simulation Results

The malfunctioning conditions are modelled by employing the coupled thermodynamics and crankshaft dynamics model in accordance to the the procedure described in Section 2. As a result of these conditions, the changes in the in-cylinder pressure of the affected cylinder are shown in Figure 4a. In addition, changes in the ICT

 https://doi.org/10.24868/issn.2515-818X.2020.033

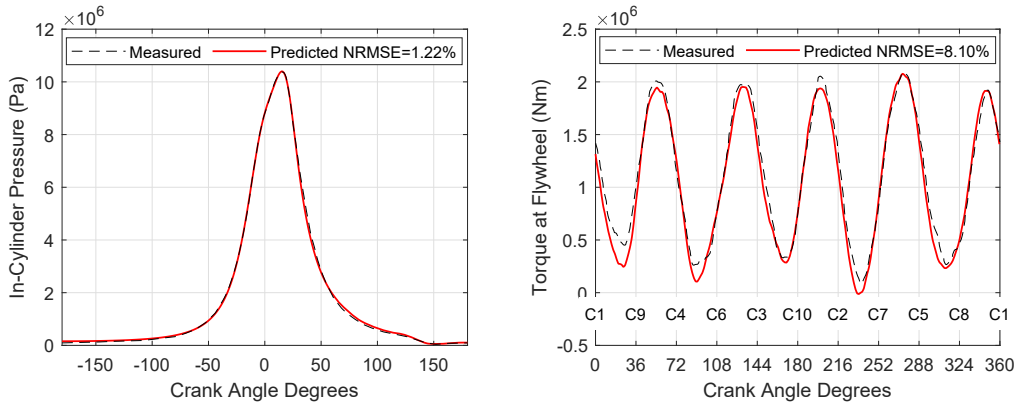

Figure 3: Engine coupled thermodynamics and crankshaft dynamics model output for 100% engine load. Firing cylinders are marked as C1, C2...C10 on the engine ICT graph.

due to the malfunctioning conditions introduced in cylinder no. 5 are shown in Figure 4b as a representative case, and the difference in torque is normalised with respect to the average torque of the baseline.

For the change in SOI, it is observed that the in-cylinder peak pressure decreases as the injection timing is retarded. This is caused as the combustion occurs in a rapidly expanding volume, which might subsequently cause a deterioration in the engine efficiency. On the contrary, as the injection timing gets too advanced, the peak pressure increases owing to the earlier start of combustion. When changes in SOI are introduced, the ICT is observed to change rapidly within 14°CA from cylinder no. 5 Top Dead Center (TDC). Among all five runs for this malfunctioning condition, the ICT is observed to changed rapidly within an average of 5°CA after the peak pressure in cylinder 5 is achieved. Specifically, it is observed that for the simulation runs where the in-cylinder pressure is greater than the baseline, the ICT increases rapidly, and the opposite holds when the in-cylinder pressure is less than the baseline. Moreover, this rapid change in ICT gets attenuated throughout the rest of the engine revolution until cylinder no. 5 fires again, which re-introduces the rapid change in the engine shaft torque. This effect, as well as the 5° delay mentioned above are caused due to the crankshaft's flexibility, which slows down the torque transmission from the firing cylinder to where the ICT is measured at the flywheel.

The change in RHR appears to have a similar effect in the in-cylinder pressure diagram as the change in SOI. In specific, the cylinder maximum pressure increases and peaks earlier in the cycle as the Weibe parameter decreases. The effects that this has on the ICT are similar to those of the change in SOI, only instead more pronounced.

The change in scavenge air pressure primarily affects the compression part of the cycle. This is especially visible in the area near the TDC where the maximum compression takes place, and the changes of the in-cylinder pressure diagram appear to be the greatest. In addition, part of the combustion is also effected, which results to a maximum change in the peak pressure of about 8 bar. Therefore, small changes in the scavenge air pressure can result to larger changes in the peak pressure, which underpins the importance of proper maintenance in the scavenge air system. This change however appears to have the smallest effect in the ICT compared to the other malfunctioning conditions. Most importantly, since the change in scavenge air pressure affects all cylinders evenly, there is not a significant change in ICT oscillations after cylinder no. 5 fires. It should also be noted that, a decrease of 0.2 bar in the scavenge air pressure at the same load, reduces the average torque of the engine by 0.5%.

Finally, the leaking exhaust valve causes a decrease in the entire in-cylinder pressure corresponding to the compression, combustion and expansion phases. As expected, the greatest changes in the in-cylinder pressure appear to take place near the peak pressure position. When compared to the change in SOI and RHR, the effect in the peak pressure is not as large. However, since the entire pressure diagram is affected, it is observed that this has a significant impact on the ICT. Since the in-cylinder pressure with a leaking exhaust valve never exceeds the baseline, the ICT amplitude decreases significantly for all simulation runs at 26°CA after the cylinder no. 5 fires, whilst the phase of the ICT signal remains unchanged in contrast to all other cases.

 https://doi.org/10.24868/issn.2515-818X.2020.033

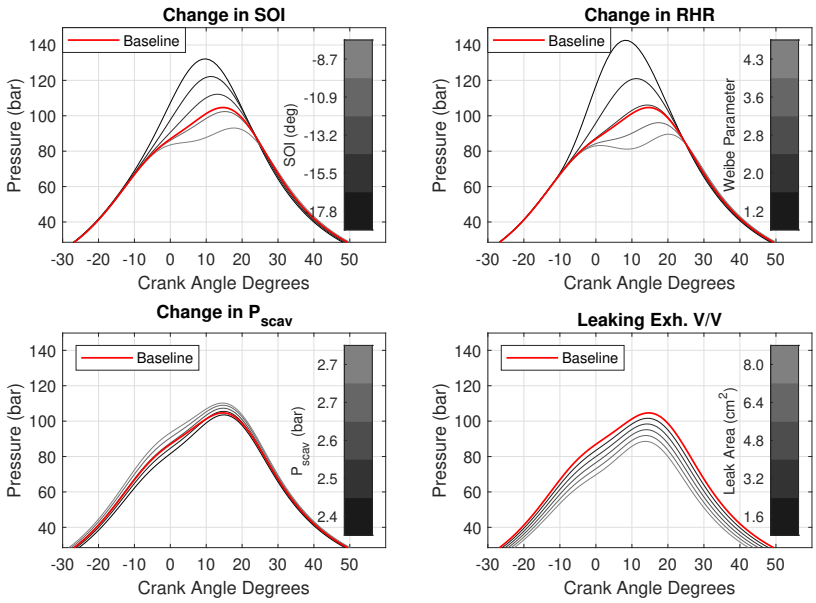

(a)

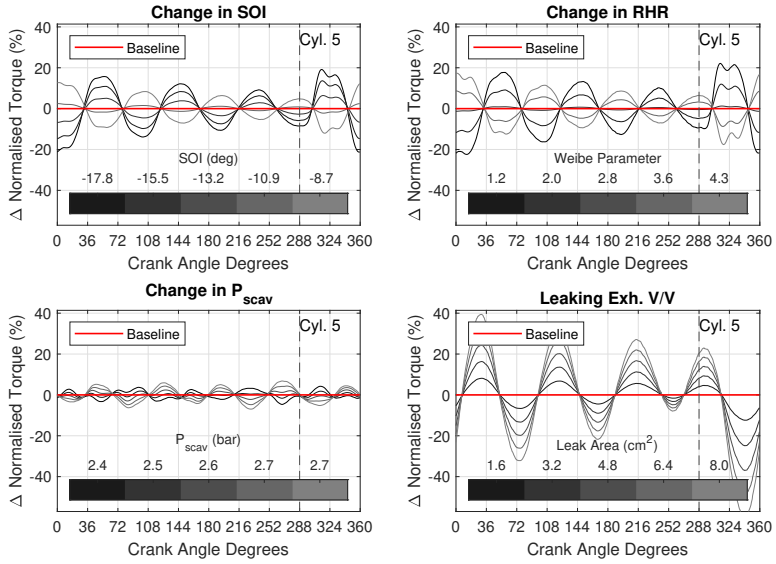

(b)

Figure 4: (a) In-cylinder pressure at malfunctioning conditions. (b) In-cylinder torque with malfunctioning condition introduced in cylinder 5.

4.3 Frequency Analysis Malfunctioning Conditions Mapping

In accordance to the followed methodology, a frequency analysis is conducted by employing a discrete Fourier transform on the ICT signals shown in Figure 4b. Using the same representative case of cylinder no. 5 as above, the engine orders mostly affected by a change in SOI are shown in Figure 5. In specific, the greatest change in modulus takes place for the 4^{th} and 12^{th} engine orders.

By performing the same procedure for all cylinders and all malfunctioning conditions, the results are shown in Figure 6. Firstly, it is observed that when any malfunctioning condition is introduced in the cylinders except for the scavenge air pressure change, the 4^{th} engine order will always be affected. Secondly, the change in scavenge air pressure results to changes in the 3^{rd}, 5^{th} and 6^{th} engine orders for all cylinders. The effect of this malfunctioning condition is therefore distinct from any other malfunctioning conditions, so it can be identified easily by employing frequency analysis as in this study. Furthermore, the leaking exhaust valve when introduced for cylinders 1-8 and 9-10, affects the 9^{th} and 2^{nd} engine orders, respectively. Similar to the scavenge air pressure change, the effect

 https://doi.org/10.24868/issn.2515-818X.2020.033

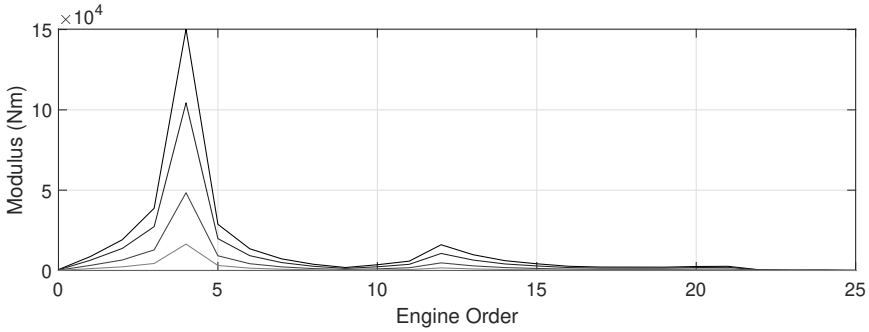

Figure 5: Frequency analysis of the ICT difference with the baseline, for changes in SOI implemented on cylinder no. 5.

of the leaking exhaust valve on these engine orders is distinct from any other malfunctioning conditions, which makes it easily identifiable. Finally, the 12th engine order is affected primarily by the change in SOI and RHR. These two malfunctioning conditions seem to be affecting the same engine orders, therefore making it harder to distinguish between the two by considering just the frequency analysis. This is expected, since the effect of these two conditions on the in-cylinder pressure diagram is very similar, as shown in Figure 4a.

Finally for the the change in SOI and RHR malfunctioning conditions, when introduced in cylinders 1,3,4,6,9 and 10, the 21st engine order is the only one that gets distinctly affected. However, it is uncertain whether this will be distinguishable in the case of field measurements due to the expected measurement noise and uncertainties.

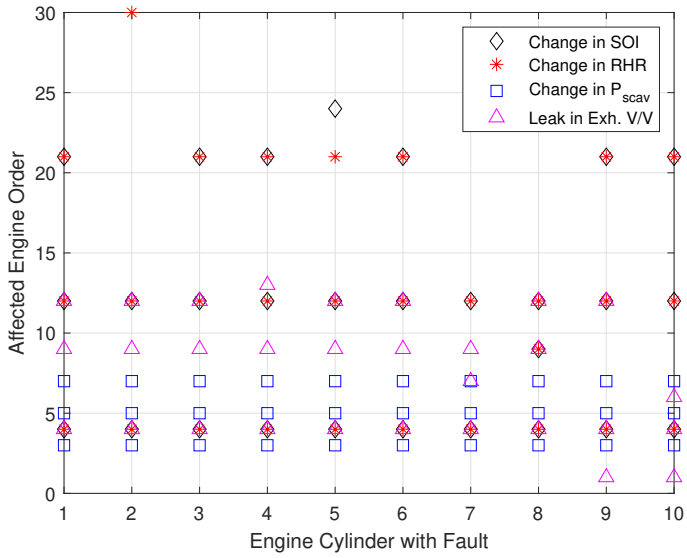

Figure 6: Engine orders affected by malfunctioning conditions.

5 Conclusions

A framework for large two-stroke diesel engine performance assessment was provided by mapping the relationship of specific malfunctioning engine conditions with the engine ICT. This was accomplished by a coupled thermodynamics and crankshaft dynamics model, where four malfunctioning conditions were simulated.

From this framework, it was established that by considering the first and second malfunctioning conditions, which were modelled as changes in SOI and RHR, identical frequency components were affected on the engine ICT. This is due to the similar effect that these malfunctioning conditions exhibited on the in-cylinder pressure. Therefore, this renders the diagnosis of any or both of these conditions possible for any cylinder, however without being able to distinguish between each other.

Regarding the third and fourth malfunctioning conditions, which were modelled as changes in the scavenge air pressure and exhaust valve leakage, there were distinct frequencies affected in the engine ICT, for all individual cylinders. This demonstrates firstly the importance of an analysis of such nature, and secondly the usefulness of the ICT measurement for diagnostic purposes. Therefore, important information on the condition of individual

 https://doi.org/10.24868/issn.2515-818X.2020.033

cylinders can be obtained by using only a single sensor (ICT measurement).

For future research, the effect of multiple combinations of failures, occurring in multiple cylinders simultaneously will be investigated. In addition, an approach will be considered to determine specific parameters of the in-cylinder pressure diagram by employing an inverse crankshaft dynamics model. This way an even better insight and understanding will be provided for the individual cylinders condition.

Abbreviations

ICT	Instantaneous Crankshaft Torque
NRMSE	Normalised Mean Square Error
RHR	Rate of Heat Release
SOI	Start of Injection
TDC	Top Dead Center
VIT	Variable Injection Timing

Acknowledgement

The authors from MSRC greatly acknowledge the funding from DNV GL AS and RCCL for the MSRC establishment and operation. Additionally, the authors gratefully acknowledge the financial support of Innovate UK, through the Knowledge Transfer Partnership project (project number 11577), for the work reported in this paper.The opinions expressed herein are those of the authors and should not be construed to reflect the views of Innovate UK, DNV GL AS and RCCL.

References

Anantharaman, M., Garaniya, V., Khan, F., Lewarn, B., 2015. Marine engines and their impact on the economy, technical efficiency and environment. Marine Engineering 50, 360–367.

Benvenuto, G., Campora, U., 2007. Performance prediction of a faulty marine diesel engine under different governor settings, in: International Conference on Marine Research And Transportation, pp. 35–44.

Cai, C., Weng, X., Zhang, C., 2017. A novel approach for marine diesel engine fault diagnosis. Cluster Computing 20, 1691–1702.

Espadafor, F.J.J., Villanueva, J.A.B., Guerrero, D.P., García, M.T., Trujillo, E.C., Vacas, F.F., 2014. Measurement and analysis of instantaneous torque and angular velocity variations of a low speed two stroke diesel engine. Mechanical Systems and Signal Processing 49, 135–153.

Guan, C., Theotokatos, G., Chen, H., 2015. Analysis of two stroke marine diesel engine operation including turbocharger cut-out by using a zero-dimensional model. Energies 8, 5738–5764.

Guerrero, D.P., Jiménez-Espadafor, F.J., 2019. Torsional system dynamics of low speed diesel engines based on instantaneous torque: application to engine diagnosis. Mechanical Systems and Signal Processing 116, 858–878.

Heywood, J.B., 1988. Internal combustion engine fundamentals. McGraw-Hill.

Hountalas, D.T., 2000. Prediction of marine diesel engine performance under fault conditions. Applied thermal engineering 20, 1753–1783.

Isermann, R., 2006. Fault-diagnosis systems: an introduction from fault detection to fault tolerance. Springer Science & Business Media.

Johnson, H., Andersson, K., 2014. Barriers to energy efficiency in shipping. WMU Journal of Maritime Affairs 15, 79–96. doi:10.1007/s13437-014-0071-z.

Kouremenos, D., Hountalas, D., 1997. Diagnosis and condition monitoring of medium-speed marine diesel engines. Tribotest 4, 63–91.

Lamaris, V., Hountalas, D., 2010. A general purpose diagnostic technique for marine diesel engines–application on the main propulsion and auxiliary diesel units of a marine vessel. Energy conversion and management 51, 740–753.

Lambrou, M., Watanabe, D., Iida, J., 2019. Shipping digitalization management: conceptualization, typology and antecedents. Journal of Shipping and Trade 4. doi:10.1186/s41072-019-0052-7.

Larsson, S., Schagerberg, S., 2004. SI-engine cylinder pressure estimation using torque sensors. Technical Report. SAE Technical Paper.

MAN B&W, . Instruction Book 'Operation' for 46-108MC/MC-C engines. Hyundai-MAN B&W.

MAN Energy Solutions, 2018. Basic principles of ship propulsion. URL: https://marine.man-es.com/docs/librariesprovider6/test/5510-0004-04_18-1021-basic-principles-of-ship-propulsion_web_links.pdf?sfvrsn=12a35ba2_30. Accessed 21 Jul. 2018.

Martyr, A.J., Plint, M.A., 2012. Engine testing: The design, building, modification and use of powertrain test facilities. Elsevier.

Matulić, N., Radica, G., Nižetić, S., 2019. Engine model for onboard marine engine failure simulation. Journal of Thermal Analysis and Calorimetry 141, 119–130. doi:10.1007/s10973-019-09118-3.

Merker, G.P., Schwarz, C., Stiesch, G., Otto, F., 2005. Simulating Combustion: Simulation of combustion and pollutant formation for engine-development. Springer Science & Business Media.

Mesbahi, E., Arriagada, J., Assadi, M., Ghorban, H., 2004. Diesel engine fault diagnosis by means of anns: A comparison of two methods, in: Proceeding of the institute of marine engineering, science and technology. Part B, journal of marine design and operations, pp. 29–37.

Rakopoulos, C., Giakoumis, E., 2007. Prediction of friction development during transient diesel engine operation using a detailed model. International journal of vehicle design 44, 143–166.

Raptodimos, Y., Lazakis, I., 2018. Using artificial neural network-self-organising map for data clustering of marine engine condition monitoring applications. Ships and Offshore Structures 13, 649–656.

Schagerberg, S., McKelvey, T., 2003. Instantaneous crankshaft torque measurements-modeling and validation. Technical Report. SAE Technical Paper.

The Swedish Club, 2018. Main engine damage. Online. Göteborg, Sweden.

Thor, M., Egardt, B., McKelvey, T., Andersson, I., 2014. Using combustion net torque for estimation of combustion properties from measurements of crankshaft torque. Control Engineering Practice 26, 233–244.

Tsitsilonis, K.M., Theotokatos, G., 2018. A novel systematic methodology for ship propulsion engines energy management. Journal of cleaner production 204, 212–236.

Tsitsilonis, K.M., Theotokatos, G., Xiros, N., Habens, M., 2020. Systematic investigation of a large two-stroke engine crankshaft dynamics model. Energies 13, 2486.

Watzenig, D., Sommer, M., Steiner, G., 2009. Engine state monitoring and fault diagnosis of large marine diesel engines. e & i Elektrotechnik und Informationstechnik 126, 173–179.

Woodyard, D., 2009. Pounder's marine diesel engines and gas turbines. Butterworth-Heinemann.

Woschni, G., 1967. A universally applicable equation for the instantaneous heat transfer coefficient in the internal combustion engine. Technical Report. SAE Technical paper.

 https://doi.org/10.24868/issn.2515-818X.2020.033